Journal of Power Sources 196 (2011) 7435–7441

Contents lists available at ScienceDirect

Journal of Power Sources

journal homepage: www.elsevier.com/locate/jpowsour

Compatibility of $La_{26}O_{27}(BO_3)_8$ electrolyte with standard cathode materials for use in proton conducting solid oxide fuel cells

K.V. Kravchyk*, E. Quarez, M. Caldes, A. Le Gal La Salle, O. Joubert

Institut des Matériaux Jean Rouxel (IMN), Université de Nantes, CNRS, 2, rue de la Houssinière, BP 32229, 44322 Nantes Cedex 3, France

ARTICLE INFO

Article history:
Received 4 March 2011
Received in revised form 18 April 2011
Accepted 19 April 2011
Available online 28 April 2011

Keywords:
$La_{26}O_{27}(BO_3)_8$
Solid oxide fuel cells
Proton conductivity
Compatibility
AC impedance

ABSTRACT

The chemical and mechanical compatibility of proton conducting $La_{26}O_{27}(BO_3)_8$ (LBO) electrolyte with standard cathode materials $La_{0.7}Sr_{0.3}MnO_3$ (LSM), $La_{0.75}Sr_{0.25}Cr_{0.5}Mn_{0.5}O_3$ (LSCM), La_2NiO_4 and $Ba_{0.5}Sr_{0.5}Co_{0.8}Fe_{0.2}O_3$ (BSCF) was investigated. The results show that LSM, LSCM and La_2NiO_4 cathodes are chemically and mechanically stable with the LBO electrolyte, and BSCF reacts with LBO after heat-treatment of their mechanical ground mixtures at $T = 1150\,^{\circ}C$. Symmetrical cell tests based on LBO demonstrated that the values of the cathode ASR (area specific resistance) are much lower in the case of the LSM and La_2NiO_4 cathodes than in the case of the LSCM cathode (in humidified air at 700 °C: $ASR_{LSM} = 15\,\Omega\,cm^2$; $ASR_{LSCM} = 60\,\Omega\,cm^2$; $ASR_{La_2NiO_4} = 1\ \ \Omega\ \ cm^2$). The large value obtained for LSCM cathode may be related to the low level of its oxygen ion conductivity. Finally, a composite cathode (CER–CER) approach was used in order to optimize the polarization resistance of the LSM cathode. Several CER–CER cathodes with different cathode/electrolyte weight ratios were prepared. The lowest value of ASR for LSM-based composite cathode was obtained by adding 50 wt.% of LBO to LSM cathode ($ASR_{LSM/LBO} = 3.4\,\Omega\,cm^2$ in humidified air at 700 °C).

1. Introduction

High temperature proton conducting materials are studied very actively nowadays as alternative electrolyte materials for solid oxide fuel cells (SOFC). The fuel cells based on proton conducting materials (PCFC) have higher theoretical electromotive force (EMF) and higher electrical efficiency than SOFC [1] due to the absence of water dilution, the water production taking place at the air side of the cell and thus there is no requirement for fuel management. These advantages increase the efficiency of PCFC by increasing the fuel utilization and by decreasing the complexity of the cell and by extension of the stack and the balance of plant. Despite the benefits of the PCFC technology, its progress is much delayed compared with SOFC. Namely, peak power density superior to $1.0\,W\,cm^{-2}$ at intermediate temperatures (600–800 °C) is frequently reported in the literature for SOFC with thin film electrolytes [2–4], while the power density of PCFC seldom exceeds $500\,mW\,cm^{-2}$ [5]. In other words, fuel cells based on proton conductors do not exhibit high performance values which are in principle thermodynamically reachable. One of the reasons is the absence of chemically and mechanically compatible electrode materials with proton conducting electrolytes. To operate for an acceptable period of time, solid oxide fuel cells need to be built with materials that have good chemical compatibility between them, and in particular at the anode/electrolyte and cathode/electrolyte interfaces. Between the anode and electrolyte materials, the compatibility is more obvious as the anode material is generally a composite based on the electrolyte material. The cathode material used is a mixed ionic–electronic conductor for which chemical and mechanical compatibility with electrolyte is essential to assure good performances and a significant lifetime of the fuel cell.

In this work, we studied potential cathode materials from chemical, mechanical and electrochemical point of view for use with the recently discovered lanthanum oxyborate $La_{26}O_{27}(BO_3)_8$ (LBO) [6,7] which reacts with water vapour to form the fully hydrated proton conducting phase $La_{26}O_{26}(OH)_2(BO_3)_8$ stable up to 700 °C. Although the latter shows lower proton conductivity ($\sigma = 6 \times 10^{-4}\,S\,cm^{-1}$ at $T = 600\,^{\circ}C$ [6]) than perovskite-type materials such as doped barium cerates ($\sigma = 1 \times 10^{-2}\,S\,cm^{-1}$ at $T = 600\,^{\circ}C$ [8]), its long-term chemical stability and low sintering temperature compared with perovskite-type materials make it a promising candidate for PCFC [9].

Based on the literature data, several cathode materials ($La_{0.7}Sr_{0.3}MnO_3$ (LSM), $La_{0.75}Sr_{0.25}Cr_{0.5}Mn_{0.5}O_3$ (LSCM) and La_2NiO_4) have been selected to test their compatibility with the lanthanum oxyborate. They exhibit close thermal expansion coefficients ($TEC_{LSM} = 11.7 \times 10^{-6}\,K^{-1}$ [10]; $TEC_{LSCM} = 12 \times 10^{-6}\,K^{-1}$ [11]; $TEC_{La_2NiO_4} 13 \times 10^{-6}\ \ K^{-1}$ [12]) with the lanthanum oxyb-

* Corresponding author. Tel.: +33 0240373929; fax: +33 0240373929.
E-mail address: Kostiantyn.Kravchyk@cnrs-imn.fr (K.V. Kravchyk).

0378-7753/$ – see front matter.
doi:10.1016/j.jpowsour.2011.04.041

orate ($TEC_{LBO} = 8.2 \times 10^{-6}\,K^{-1}$ [9]) and they are all mixed ion/electron (hole) conductors. To highlight the importance of the TEC discrepancy between the electrolyte and the cathode, $Ba_{0.5}Sr_{0.5}Co_{0.8}Fe_{0.2}O_3$ (BSCF) was also chosen as cathode candidate ($TEC_{BSCF} = 20 \times 10^{-6}\,K^{-1}$ [13]).

Based on obtained results, the most potential half cell architectures (lanthanum oxyborate-cathode) were identified according to the chemical and mechanical compatibility between electrolyte and cathodes and their electrochemical behaviors.

2. Experimental

The synthesis of the $La_{26}O_{27}(BO_3)_8$ was carried out by precipitation from solution method. Aqueous solutions of $La(NO_3)_3$, $B(OH)_3$ and NH_4OH were used as initial reagents. All used reactants were of analytical reagent grade. Lanthanum hydroxide was precipitated at pH 8.5 by water ammoniac solution and washed with distilled water until Cl^- and NO^{3-} ions disappeared in the washing solutions. Afterwards an appropriate amount of the aqueous solution of $B(OH)_3$ was added in order to obtain the chemical composition $La_{26}O_{27}(BO_3)_8$. Then the suspension was homogenized during 6 h in a ball-milling apparatus using zirconium balls and distilled water. The homogenized mixture was then dried at 100 °C and annealed at $T = 1100$ °C for 2 h in air.

La_2NiO_4 was prepared via the traditional solid-state reaction method. Pre-dried stoichiometric amounts of La_2O_3 and NiO oxides were milled for 30 min in a ball-milling apparatus using ethanol as a solvent and then heat-treated at $T = 1100$ °C for 4 h.

The BSCF powders were synthesized by self-combustion method. $Ba(NO_3)_2$, $Sr(NO_3)_2$, $Co(NO_3)_2{\cdot}6H_2O$, $Fe(NO_3)_3{\cdot}9H_2O$, all in analytical grades, were used as raw materials and glycine was used as the chelating agent. Stoichiometric amounts of metal nitrates were dissolved into a water solution. Afterwards the required amount of glycine was added into the solution under stirring. The mixed solution was then heated at 80 °C on a hot plate under constant stirring for 4–5 h until a gel was formed. One hour later the precursor powder of BSCF was formed by self-combustion of the gel. The obtained powder was then annealed at $T = 1000$ °C for 10 h in order to obtain the BSCF powder.

The LSM and LSCM powders were provided by Praxair (France).

The XRD patterns of electrolyte, cathode and electrolyte/cathode powders were recorded at room temperature using Siemens D5000 diffractometer (Cu Kα1: λ = 1.54060 Å, Cu Kα2: λ = 1.54439 Å). The refinements of the cell parameters were carried out using the program FULLPROF [14] in the full pattern matching mode with the program WinPLOTR interface [15]. The XRD patterns of synthesized and provided powders (LBO, LSM, LSCM, La_2NiO_4 and BSCF) confirmed the absence of any impurity phases (Fig. 1).

In order to check chemical compatibility between $La_{26}O_{27}(BO_3)_8$ and LSM, LSCM, La_2NiO_4, the electrolyte/cathode mixtures with 1:1 weight ratio were ground together, pressed into pellets and annealed at 1150 °C for 36, 72 and 144 h in air. The stability under wet air was checked by annealing the electrolyte–cathode mixtures at 700 °C under $pH_2O = 0.025$ atm for 36 h.

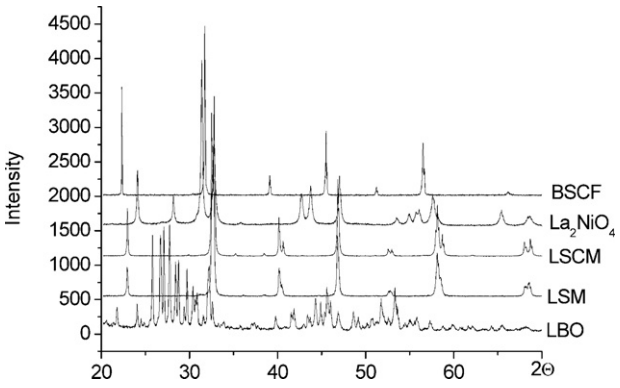

Fig. 1. XRD patterns of LBO, LSM, LSCM, La_2NiO_4 and BSCF compounds measured at room temperature used in the present study.

Dense ceramics were obtained by uniaxial compression of $La_{26}O_{27}(BO_3)_8$ powders, followed by a heat treatment at 1240 °C during 4 h. The pellets were then polished with fine abrasives down to ~0.3 mm thickness, and slurries of cathode materials were coated on the surface by screen printing. The symmetrical cells were subsequently annealed at 1150 °C for 36 h, with heating and cooling rates about 150 °C h^{-1}. The microstructure and element analysis of the obtained products were studied by SEM imaging and EDS analysis using a scanning electron microscope (JEOL JSM 7600) equipped with a germanium X-ray detector. Porosity of the sintered cathode layers was estimated for the SEM images using Image Tool program.

The AC impedance spectra were collected in air by a Solartron 1260 impedance analyzer over the frequency range 0.1 Hz–1 MHz, in the temperature range 200–850 °C upon cooling and heating, by steps of 50 °C, with isotherm of 1 h at each step. The analysis of the impedance spectra was carried out using the program Zview [16].

3. Results and discussion

Fig. 2 shows X-ray powder diffraction (XRPD) patterns of LBO–LSM, LBO–LSCM, LBO–La_2NiO_4 and LBO–BSCF mixtures collected at room temperature before and after the thermal-treatment at $T = 1150$ °C for 36, 72 and 144 h under air and at $T = 700$ °C for 36 h under wet air ($p_{H_2O} = 0.023$ atm) compared with the XRPD of the LBO alone. Table 1 gathered the unit cell volume for the corresponding phases. Similar observations (Fig. 2a, b, and d) can be done for the mixture of LBO and LSM, LSCM and La_2NiO_4 cathodes: the absence of chemical reactions after heat-treatment in air at $T = 1150$ °C and wet air at $T = 700$ °C. This is confirmed in Table 1, where no significant changes of unit cell volume were observed for LBO, LSM, LSCM and La_2NiO_4 phases in cathode–electrolyte mixtures. Small shift of LBO peaks, as well as appearance of new small ones and changes of unit cell volumes of LBO phase after heat-treatment can be due to the variation of its hydration state ($V_{dry\ La_{26}O_{27}(BO_3)_8} = 1288.8(3)$ Å^3 in dry state; $V_{wet\ La_{26}O_{26}(OH)_2(BO_3)_8} = 1299.9(5)$ Å^3 in wet state) [6]. Studies of LBO–BSCF mixtures (Fig. 2c) showed that after annealing at $T = 1150$ °C reaction takes place between both components lead-

Table 1
Unit cell volumes of LBO, LSM, LSCM and La_2NiO_4 phases in the LBO/LSM, LBO/LSCM and LBO/La_2NiO_4 mixtures before and after heat treatment at $T = 1150$ °C for 36 h in air.

Mixture	V (Å^3) of LBO before heat treatment	V (Å^3) of LBO after $T = 1150$ °C for 36 h in air	V (Å^3) of cathode before heat treatment	V (Å^3) of cathode after $T = 1150$ °C for 36 h in air
LSM/LBO	1290.7(1)	1292.4(6)	350.5(2)	350.5(7)
LSCM/LBO	1289.7(3)	1291.2(1)	350.1(3)	350.4(5)
La_2NiO_4/LBO	1290.8(8)	1293.1(3)	189.4(3)	189.5(4)

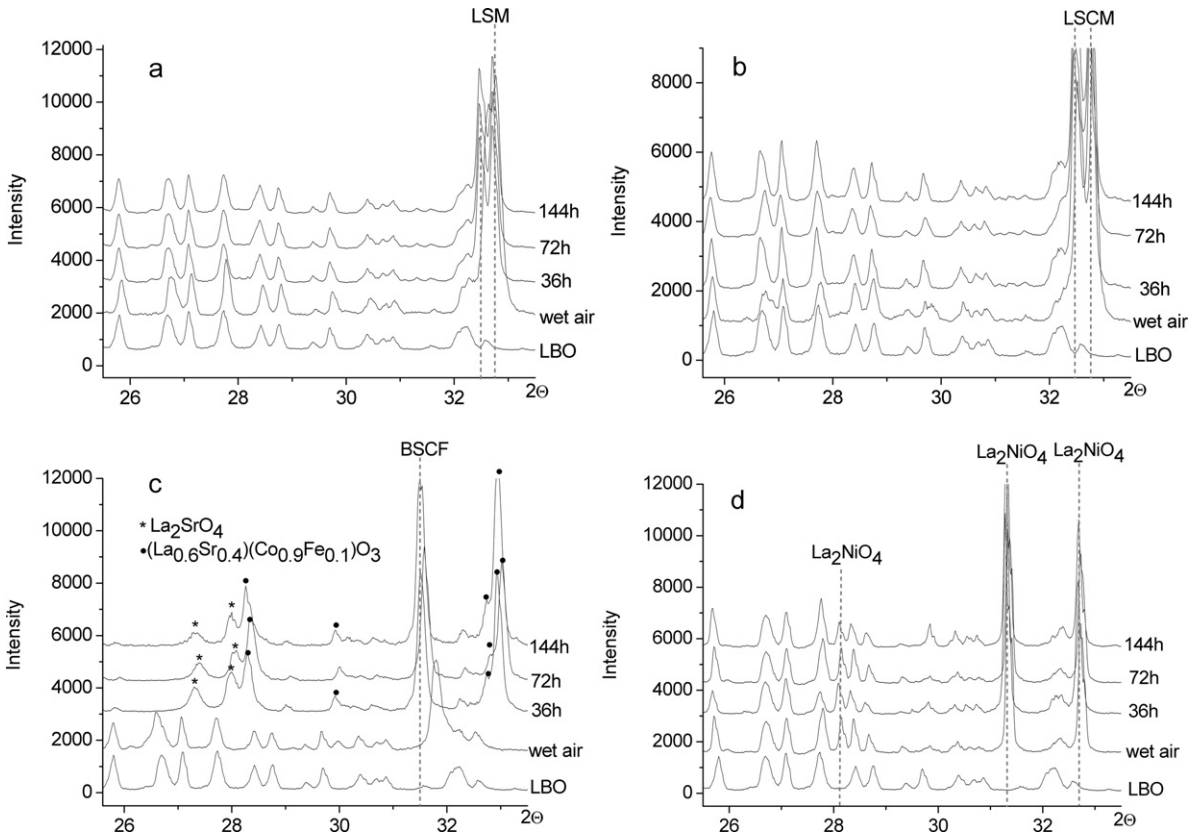

Fig. 2. XRD patterns of LBO–LSM (a), LSCM (b), BSCF (c) and La_2NiO_4 (d) mixtures measured at room temperature after heat treatment at $T = 700\,^{\circ}C$ for 36 h in wet air ($pH_2O = 0.025$ atm) and at $T = 1150\,^{\circ}C$ for 36, 72, 144 h in air. XRD patterns of pure LBO phase are given for comparison.

ing mainly to the formation of $La_{0.6}Sr_{0.4}Co_{0.9}Fe_{0.1}O_3$ (LSCF) and La_2SrO_4 phases, whereas at lower temperature (700 °C) in wet air no chemical reaction is observed.

Cross-sections of the LSM, LSCM and La_2NiO_4 cathodes screen-printed on LBO electrolyte sintered at $T = 1150\,^{\circ}C$ for 2 h are shown in Fig. 3a–c, respectively. The cathode layers were about 18 μm thick, sufficiently porous (see Table 2) and exhibited good interface with the lanthanum oxyborate electrolyte, with no sign of crack or delamination. It is in good agreement with available thermal expansion data for the investigated compounds (Table 3). It

Table 2
Porosity of LSM, LSCM, La_2NiO_4 and composite LBO/LSM (50 wt.% of LBO) cathode layers.

Cathode	Porosity (%)
La_2NiO_4	18
LSM	19
LSCM	41
LBO/LSM	13

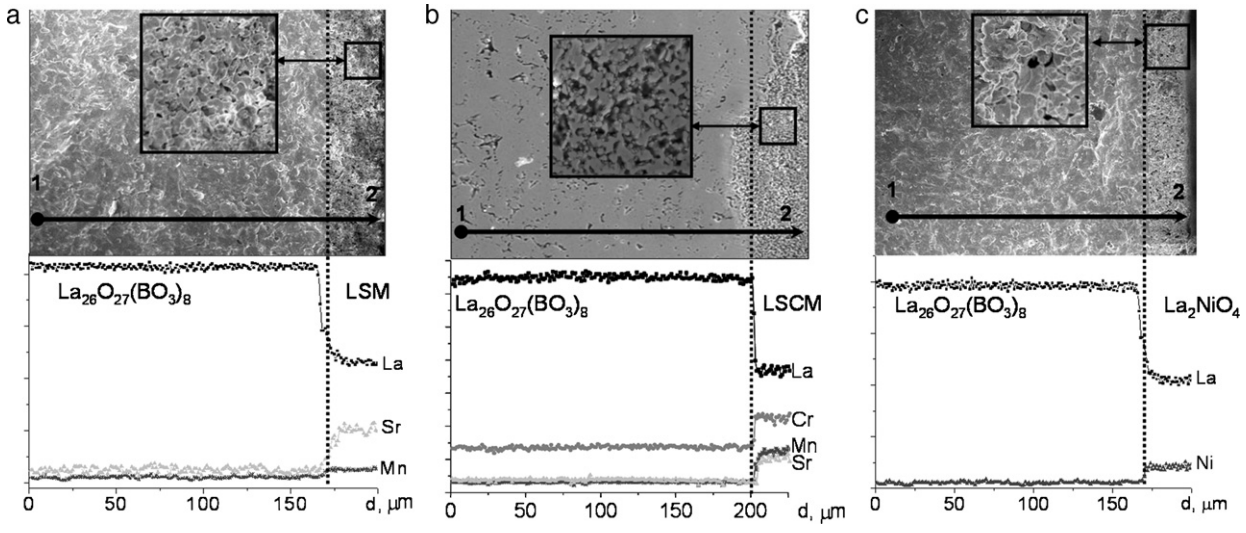

Fig. 3. Typical fracture cross-section SEM images and backscattered electron micrographs of LSM (a), LSCM (b) and La_2NiO_4 (c) diffusion couples screen-printed on the LBO surface and heat-treated at $T = 1150\,^{\circ}C$ for 36 h.

Table 3
Linear thermal expansion coefficients for the used electrolyte and cathode materials.

Compound	TEC × 10^{-6} (K^{-1})	Reference
LBO	8.2	[9]
LSM	11.7	[10]
LSCM	12	[27]
La_2NiO_4	13	[12]
BSCF	20	[13]

is worth noting that the several attempts to prepare symmetrical cells based on BSCF cathode were always sanctioned by cathode delamination. This is probably related to the large TEC discrepancy ($TEC_{LBO} = 8.2 \times 10^{-6}\ K^{-1}$ [9], $TEC_{BSCF} = 20 \times 10^{-6}\ K^{-1}$ [13]) or the presence of chemical reaction between LBO and BSCF. The electrolyte layer is well densified and shows an average grain size of 2–4 μm (Fig. 4). The LSCM cathode showed smaller particle sizes with a homogeneous particle size distribution and larger porosity in comparison with LSM and La_2NiO_4 cathodes. Compositional analysis carried out by EDS method on the interface area, confirmed a clear phase boundary and the absence of any cation diffusion between electrolyte and cathodes in the LSM, LSCM, La_2NiO_4–LBO symmetrical cells (Fig. 3a–c).

Fig. 5a presents typical impedance diagrams for symmetrical cells based on LBO with LSM, LSCM and La_2NiO_4, plotted in the Nyquist plane, and recorded at $T = 700\,^{\circ}C$ in wet air. The impedance data were fitted using an electrical equivalent circuit made of series R//CPE (Constant Phase Element) elements. As the diagrams display two separated semi-circles at $T = 700\,^{\circ}C$, two serial (R//CPE) elements were used to fit the impedance diagrams. As a result, for all symmetrical cells, capacitance of about 10^{-9} F was observed for the first semicircle at high frequency which can be attributed to the grain boundary resistance of the electrolyte. The second semicircle presents a higher capacitance ($C_{La_2NiO_4} = 10^{-4}$ F; $C_{LSM} = 10^{-2}$ F; $C_{LSCM} = 10^{-2}$ F) corresponding to the electrode polarization. The arc observed in the case of La_2NiO_4 is very depressed (inset Fig. 4a) suggesting that the modeling with an R//CPE circuit is perhaps not relevant. Nevertheless, our aim is to compare samples and not to give mathematical model and to go deeply into mechanism comprehension. At lower temperatures (<400 °C) a semicircle corresponding to bulk resistance of electrolyte appears (Fig. 5b) which was modelled by adding an R//CPE element to the previous equivalent circuit. As it can be seen from Fig. 5a and b, electrolyte response (grain and grain boundary resistances) is similar for all measured symmetrical cells, however, the polarization resistance

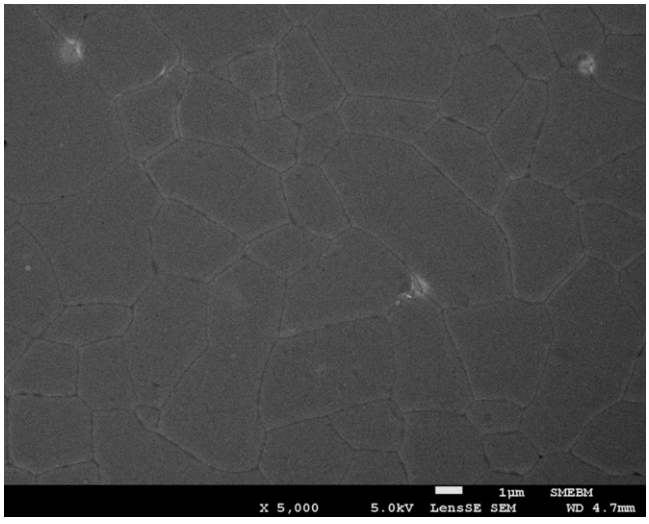

Fig. 4. Microstructure of ceramic LBO electrolyte sintered at 1240 °C for 4 h.

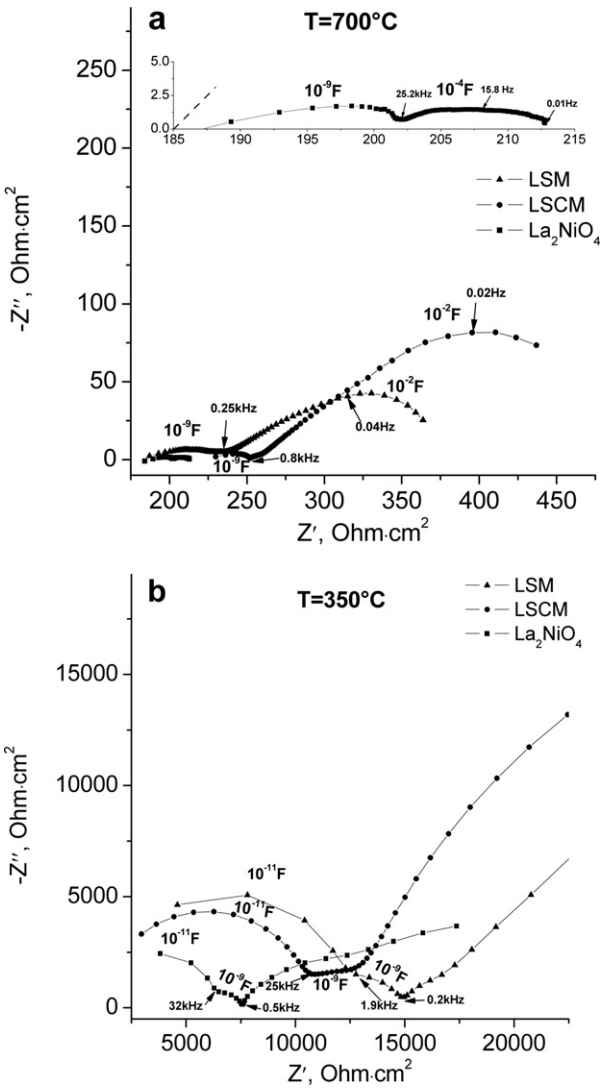

Fig. 5. Impedance spectra of LSM/LBO/LSM, LSCM/LBO/LSCM and La_2NiO_4/LBO/La_2NiO_4 symmetrical cells measured at $T = 700\,^{\circ}C$ with in inset a magnification for the La_2NiO_4 case (a) and 350 °C (b) under wet air.

differs strongly depending on the cathode material. From the values of bulk and grain boundary resistances, the total conductivity of the lanthanum oxyborate electrolyte was determined. Area specific resistances were calculated from the total resistances of cathodes using the following equation:

$$ASR = \frac{R \cdot S}{2} \quad (1)$$

where R is the polarization resistance of the cathodes and S, the surface area of the electrolyte covered by cathode on one side.

Fig. 6 shows the plots of the total conductivity (grain + grain boundary) as a function of the inverse temperature for $La_{26}O_{27}(BO_3)_8$ measured with Au, LSM, LSCM and La_2NiO_4 cathodes under dry air (Au) and wet air. Under wet air below $T = 700\,^{\circ}C$, data show an increase of the conductivity in comparison with measurements in dry atmosphere. This is related to the hydration behavior and the addition of the proton conductivity to the total conductivity [6,7]. Only a slight increase of the total conductivity of $La_{26}O_{27}(BO_3)_8$ was observed with Au cathodes meaning that the resistances of electrolyte are similar and do not depend on the cathodes in the investigated temperature range. This is an important confirmation of the absence of chemical

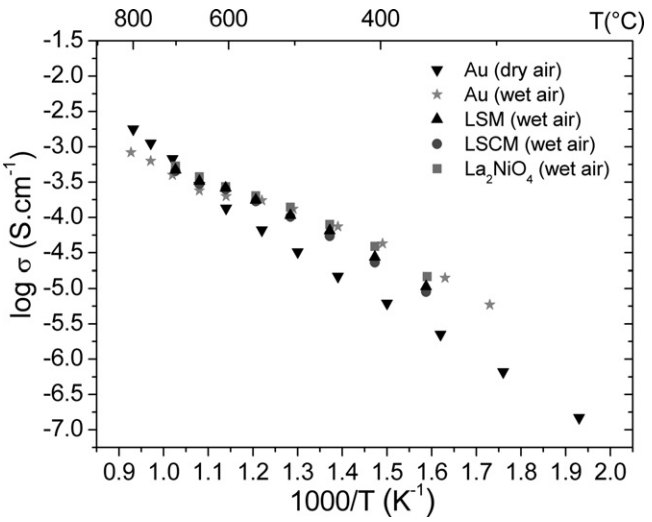

Fig. 6. Temperature dependences of total conductivity of LBO measured with Au, LSM, LSCM and La_2NiO_4 in wet air and with Au in dry air.

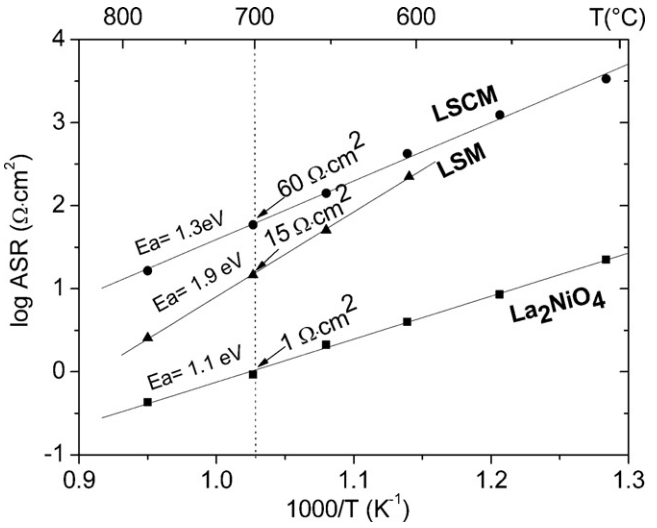

Fig. 7. Temperature dependence of area specific resistance for LSM, LSCM and La_2NiO_4 cathodes measured in symmetrical cell configuration with LBO electrolyte.

reactions between electrolyte and cathodes without any formation of intermediate phase at the interface.

Temperature dependence of area specific resistance (ASR) of LSM, LSCM and La_2NiO_4 cathodes are presented in Fig. 7. Whatever the cathode materials, an Arrhenius behavior is observed with an activation energy ranging from 1.1 to 1.9 eV, from La_2NiO_4 to LSM, respectively. The results of electrochemical behavior of symmetrical cells based on lanthanum oxyborate tested with different LSM, LSCM, La_2NiO_4 cathode materials are quite different. The lowest ASR value was obtained for La_2NiO_4 (ASR $\approx 1\ \Omega\ cm^2$ at 700 °C). For LSM and LSCM cathodes, ASR values were equal to 15 and 60 $\Omega\ cm^2$, respectively, at $T = 700$ °C.

Considering possible limiting steps determining ASR for each cathode, the following parameters should be taken into account: level of electronic, oxygen and proton conductivity, electrocatalytic activity, microstructure characteristics (i.e. porosity) and the presence of extra phase due to chemical reaction or cation diffusion between electrolyte and cathode. Taking into account that the level of electronic conductivity of LSCM is higher than that of LSM ($\sigma_{LSM} \sim 4\ S\ cm^{-1}$ [17]) and almost equivalent to the one of La_2NiO_4 ($\sigma_{LSCM} \sim 60\ S\ cm^{-1}$ [18]; $\sigma_{La_2NiO_4} \sim 80\ S\ cm^{-1}$ [19,20]) and that LSCM cathode layer is more porous than LSM and La_2NiO_4 cathodes (see Fig. 3 and Table 2), it can be concluded that electronic conductivity and microstructure are not limiting ASR parameters. The presence of extra phases lowering the performances cannot be also taken into account as no chemical reaction and chemical diffusion was observed between LBO and investigated cathodes. On the contrary, oxygen conductivity level of LSCM is relatively low compared to that of LSM and La_2NiO_4 ($\sigma_{LSCM} \sim 3 \times 10^{-5}\ S\ cm^{-1}$ [21]; $\sigma_{LSM} \sim 2 \times 10^{-3}\ S\ cm^{-1}$ [22]; $\sigma_{La_2NiO_4} \sim 2 \times 10^{-1}\ S\ cm^{-1}$ [23] at $T = 950$ °C), that means that oxygen ion transport in LSCM cathode mainly occurs via the surface pathway to the three-phase boundary sites (TPB) (Fig. 8a). However, with higher oxygen conductivity in the LSM and especially La_2NiO_4, the transport of oxygen ions also

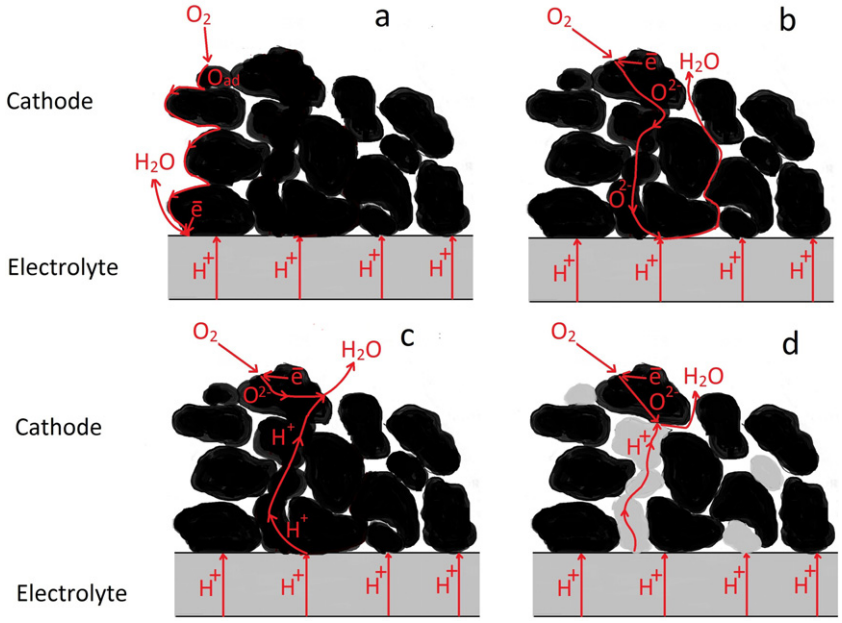

Fig. 8. Schematic diagrams of cathode-reaction mechanisms in the case of proton conducting electrolyte with: electronic conductor (a), mixed oxygen-electronic conductor (b), mixed oxygen–proton-electronic conductor (c) and mixed oxygen-electronic + proton conductors (CER–CER) (d) as cathode materials.

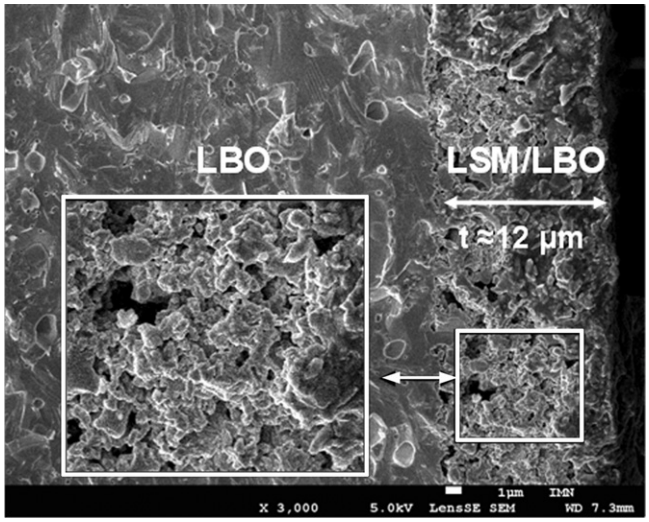

Fig. 9. Typical fracture cross-section SEM image of LBO/LSM composite cathode screen-printed on the LBO surface and heat-treated at $T = 1150\,^{\circ}C$ for 36 h.

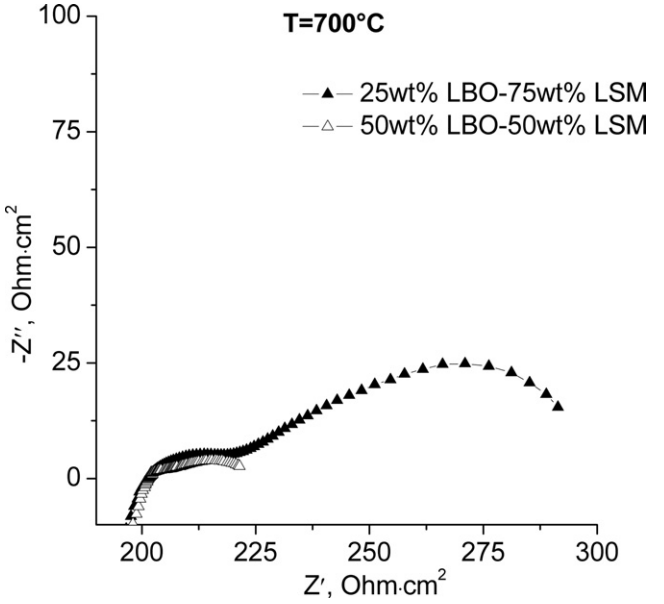

Fig. 10. Impedance spectra of LBO symmetrical cells with CER–CER (LBO–LSM) cathodes measured at $T = 700\,^{\circ}C$ under wet air.

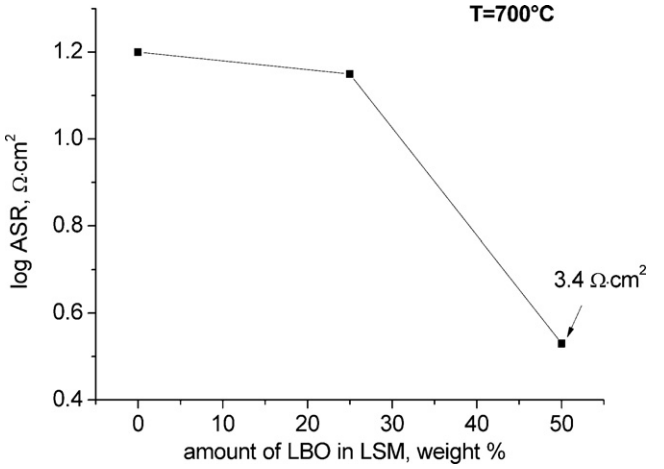

Fig. 11. Dependence of area specific resistance of LBO/LSM composite cathode measured in symmetrical cell configuration based on LBO at $T = 700\,^{\circ}C$ with the content of LBO electrolyte in the composite.

occurs via the bulk pathway (Fig. 8b). This is supposed to increase the reaction area and reduce the polarization resistance. Another important parameter is the level of proton conductivity for above-investigated cathode materials as it well known that the use of a protonic mixed conducting oxide allows the production of water not only at the TPB sites, but also over the whole cathode surface [24,25] (Fig. 8c). In this case, symmetrical cell system would obviously exhibit faster electrode processes. However, in the literature, there is no data concerning proton conductivity of LSM, LSCM and La_2NiO_4. Therefore, based on available data, the ASR decrease from LSCM to La_2NiO_4 cathodes in current symmetrical cell systems can be explained by a better oxygen conductivity level in the investigated cathodes what facilitates the oxygen ions migration through the cathode itself [26] and therefore multiply the possible reaction sites.

One way to decrease the cathode ASR is to prepare a composite cathode consisting in a mixture of a proton conductor electrolyte and a mixed O^{2-}/e^{-} conductor cathode materials. Composite cathodes provide a high density of TPBs due to the proton conducting phase in the cathode layer. Indeed, the TPBs are spread into the bulk of cathode layers what improve the diffusion and reaction of protons and oxygen species leading to ASR decrease (Fig. 8d). Thus, composite cathodes with 25, 50 and 75 wt.% (≈28, 53 and 78 vol.%) of electrolyte were prepared to improve the ASR of LSM cathode in symmetrical cells based on lanthanum oxyborate. Fig. 9 shows typical cross-sectional SEM image of LSM–LBO cathode with 50 wt.% of LBO, sintered at 1150 °C for 2 h. Generally, the LSM and LBO particles appear to be more sintered but more bonded to the LBO interface compared to pure LSM cathode. The particle size is also larger and a lower porosity is observed (Table 2). However, the shape of impedance spectra for symmetrical cells with composite (CER–CER) cathodes were very similar to that of pure LSM (Fig. 10). Thus, the fitting of the impedance diagrams was made with similar electrical equivalent circuits used for LSM cathode. Despite the porosity decrease and the particle sizes increase of the LSM-composite cathodes, the improvement of their electrochemical behavior was established. As shown in Fig. 11, ASR of cathode materials decreases with increasing weight % of lanthanum oxyborate in the composite from ≈25 to 50 wt.%. The minimum ASR is obtained for LSM–50LBO and is equal to 3.4 Ω cm^2 at $T = 700\,^{\circ}C$ which is five times lower than the one obtained for pure LSM. This confirms the positive role in reducing polarization resistance of the proton conduction in a composite cathode. CER–CER composite cathodes based on La_2NiO_4 are currently under investigation.

4. Conclusions

LSM, LSCM, La_2NiO_4 and BSCF compounds were investigated for potential application as cathode material for PCFC based on lanthanum oxyborate electrolyte. It was shown that LSM, LSCM and La_2NiO_4 cathodes are chemically and mechanically stable with the $La_{26}O_{27}(BO_3)_8$ electrolyte and that BSCF reacts with $La_{26}O_{27}(BO_3)_8$.

Conductivity measurements performed on symmetrical cells revealed that the La_2NiO_4 and LSM cathodes present the lowest values of area specific resistance (ASR) compared with those of the LSCM cathode: $ASR_{LSM} = 15\,\Omega\,cm^2$; $ASR_{LSCM} = 60\,\Omega\,cm^2$; $ASR_{La_2NiO_4} = 1\ \Omega\ cm^2$ in humidified air at 700 °C. This can be explained by a lower level of oxygen conductivity of LSCM compared to LSM and La_2NiO_4.

Optimization of the LSM cathode ASR by preparation of CER–CER composite cathodes with different cathode/electrolyte weight

ratios was performed. The lowest value of ASR for LSM-based cathode was obtained when adding 50 wt.% of LBO to LSM cathode: $ASR_{LSM} = 3.4\ \Omega\ cm^2$ in humidified air at 700 °C.

Low ASR values for La_2NiO_4 and LSM-based cathodes in $La_{26}O_{27}(BO_3)_8$ symmetrical cells make these materials potential electrolyte–cathode couples for proton-conducting solid oxide fuel cell.

Acknowledgment

This work has been performed in the frame of the FP7 Project EFFIPRO "Efficient and robust fuel cell with novel ceramic proton conducting electrolyte" (Grant Agreement 227560).

References

[1] W. Amsak, S. Assabumrungrat, P.L. Douglas, N. Laosiripojana, S. Charojrochkul, Chem. Eng. J. 119 (2006) 11–18.
[2] Z.P. Shao, S.M. Haile, Nature 431 (2004) 170–173.
[3] Q.L. Liu, K.A. Khor, S.H. Chan, J. Power Sources 161 (2006) 123–128.
[4] S.D. Kim, H. Moon, S.H. Hyun, J. Moon, J. Kim, H.W. Lee, Solid State Ionics 178 (2007) 1304–1309.
[5] Y. Lin, R. Ran, Y. Zheng, Z. Shao, W. Jin, N. Xu, J. Ahn, J. Power Sources 180 (2008) 15–22.
[6] S. Noirault, S. Celerier, O. Joubert, M.T. Caldes, Y. Piffard, Adv. Mater. 19 (2007) 867–870.
[7] S. Noirault, S. Celerier, O. Joubert, M.T. Caldes, Y. Piffard, Inorg. Chem. 46 (2007) 9961–9967.
[8] H. Matsumoto, Y. Kawasaki, N. Ito, M. Enoki, T. Ishihara, Electrochem. Solid-State Lett. 10 (2007) B77–B80.
[9] S. Noirault, Ph.D. thesis, Nantes, France, 2008.
[10] Y. Sakaki, Y. Takeda, A. Kato, N. Imanishi, O. Yamamoto, M. Hattori, M. Iio, Y. Esaki, Solid State Ionics 118 (1999) 187.
[11] J.-D. Kim, G.-D. Kim, J.-W. Moon, Y.-I. Park, W.-H. Lee, K. Kobayashi, M. Nagai, Ch.-E. Kim, Solid State Ionics 143 (2001) 379.
[12] J.M. Bassat, P. Odier, A. Villesuzanne, C. Marin, M. Pouchard, Solid State Ionics 167 (2004) 341–347.
[13] B. Wei, Z. Lu, S. Li, Y. Liu, K. Liu, W. Su, Electrochem. Solid-State Lett. 8 (2005) A428–A431.
[14] T. Roisnel, J. Rodriguez-Carvajal, Physica B 192 (1993) 55–69 (see also http://www-llb.cea.fr/fullweb/fp2k/fp2k.htm).
[15] T. Roisnel, J. Rodriguez-Carvajal, in: R. Delhez, E.J. Mittenmeijer (Eds.), Materials Science Forum, Proceedings of the 7th European Powder Diffraction Conference (EPDIC 7), 2000, pp. 118–123 (see also http://www-llb.cea.fr/fullweb/winplotr/winplotr.htm).
[16] D. Johnson, Zview Program, Version 2.8, Scribner Associates, Inc., Southern Pines, North Carlina, 1990–2002.
[17] Ch.-Ch.T. Yang, W.-Ch.J. Wei, A. Roosen, Mater. Chem. Phys. 81 (2003) 134–142.
[18] S.M. Plint, P.A. Connor, Sh. Tao, J.T.S. Irvine, Solid State Ionics 177 (2006) 2005–2008.
[19] V.V. Kharton, A.A. Yaremchenko, A.L. Shaula, M.V. Patrakeev, E.N. Naumovich, D.I. Logvinovich, J.R. Frade, F.M.B. Marques, J. Solid State Chem. 177 (2004) 26–37.
[20] S. Nishiyama, D. Sakaguchi, T. Hattori, Solid State Commun. 94 (1995) 279–282.
[21] V.V. Kharton, E.V. Tsipis, I.P. Marozau, A.P. Viskup, J.R. Frade, J.T.S. Irvine, Solid State Ionics 178 (2007) 101–103.
[22] V.V. Kharton, A.P. Viskup, I.P. Marozau, E.N. Naumovich, Mater. Lett. 57 (2003) 3017–3021.
[23] A.L. Shaula, E.N. Naumovich, A.P. Viskup, V.V. Pankov, A.V. Kovalevsky, V.V. Kharton, Solid State Ionics 180 (2009) 812–816.
[24] J. Dailly, S. Fourcade, A. Largeteau, F. Mauvy, J.C. Grenier, M. Marrony, Electrochim. Acta 55 (2010) 5847–5853.
[25] S.W. Tao, Q.Y. Wu, D.K. Peng, G.Y. Meng, J. Appl. Electrochem. 30 (2000) 153–157.
[26] J. Richter, P. Holtappels, T. Graule, T. Nakumura, L.J. Gauckler, Monatch. Chem. 140 (2009) 985–999.
[27] J.D. Kim, G.D. Kim, J.W. Moon, Y.I. Park, W.H. Lee, K. Kobayashi, et al., Solid State Ionics 143 (2001) 379–389.